

A FAST GAIN CALIBRATION ALGORITHM FOR BEAM POSITION MONITORING AT TAIWAN PHOTON SOURCE

J.Y. Chen, C.H. Chen, M.S. Chiu, P.C. Chiu, P.J. Chou, S. Fann, K.H. Hu, C.S. Huang, C.C. Kuo, T.Y. Lee, C.C. Liang, Y.C. Liu, G.H. Luo, H.J. Tsai and F.H. Tseng
National Synchrotron Radiation Research Center, Hsinchu, 30076, Taiwan

Abstract

A stable, reliable and well-calibrated beam position monitor (BPM) system is essential for the safe and precise operation of accelerators. The BPM system not only determines accelerator parameters, such as Twiss parameters, but also helps to avoid damage to accelerator components by high-energy particle beams or radiation. In this paper, we discuss a new BPM calibration scheme tested at the Taiwan Photon Source (TPS). By changing the current in a single of a horizontal or vertical corrector magnet, we generate an orbit distortion with respect to the nominal reference orbit. The difference orbit is measured at each BPM pickup location with different apertures, as a function of beam current. The raw BPM data are digitized by an analog-to-digital converter (ADC). Comparison of the beam orbit response in terms of raw ADC data from each BPM with the expected beam displacement we calibrate the beam position monitors. Moreover, because of limited setup time available after a long shutdown, this new procedure acts as a fast, easy way for BPM calibration.

INTRODUCTION

The goal of modern synchrotron light accelerators is a high brightness or a small emittance electron beam. In addition, the operation of insertion devices in modern storage rings requires accurate beam position control to, for example, avoid damage to undulator magnet arrays. Hence, a precise calibration scheme for the BPM system is needed to meet the requirements of beam quality for regular long-term operation. In this paper, we discuss a beam-based method to evaluate the relative BPM gain with the same hardware configuration. Raw BPM data signals from four pickup buttons are taken in turn-by-turn mode while the beam orbit is displaced. Depending on the associated beam pipe configuration, four types of BPMs were installed in the TPS storage ring. Two major BPM types are shown in Fig. 1. The TPS contains 24 Double Bend Achromat cells, each equipped with seven BPMs, where the 2nd ~ 6th BPM are of type-1 while the 1st and 7th BPM are of type-2.

DATA SAMPLES

In this study, we generate an orbit distortion with respect to the nominal reference orbit by changing the current in a single horizontal or vertical corrector magnet and measure the response of the orbit change at each BPM pickup location for a beam current of 15 mA. In order to ensure the correctness of data taking, a dead time

between every measurement of 3.0 seconds was chosen to provide sufficient magnet response time and turn-by-turn data refreshing.

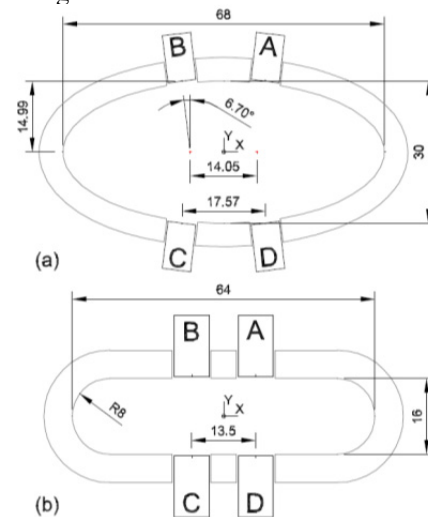


Figure 1: Cross sections of type-1 (a) and type-2 (b) BPMs installed in the TPS storage ring, where the electron beam direction is out of the paper and the length unit is millimeter.

Following the difference-over-sum processing [1], the transverse position (x, y) of the electron beam inside the vacuum chamber at the desired BPM location can be evaluated by Eq. (1) and (2).

$$x = k_x \frac{(B+C)-(A+D)}{A+B+C+D} + X_{offset} \quad (1)$$

$$y = k_y \frac{(A+B)-(C+D)}{A+B+C+D} + Y_{offset} \quad (2)$$

where

A/B/C/D	Induced voltage of each pickup button.
X_{offset}/Y_{offset}	Transverse position offset.
k_x/k_y	A dimension scale factor for (x,y) [2].

ALGORITHM

When the electron beam is close to the pickup button and/or the beam current is high, the raw BPM data response is larger. Figure 2(a) shows the highest raw BPM data response of button B while the beam position is close to -6.5 mm, where the button B is located, or -7.0 mm away from the center of the BPM as shown in Fig. 1(a). Under the same circumstance, the BPMs with the same geometry and mechanical configuration should have the same raw BPM data response. We simply overlay the raw signals from each of the four pickup buttons of BPM#5 in Fig. 2(a). The four raw BPM data signals do intersect at $X = 0$ as we expected. One step further, we mirrored the responses of button A and button D about

$X = 0$ as shown in Fig. 2(b). Figure 2(b) indicates that a well-calibrated BPM system should have identical raw BPM data responses (identical slope and vertical offset) for each pickup button in all BPMs. Within the range of closed-orbit distortions during normal accelerator operation, the raw BPM data responses are expected to have good linearity. Unfortunately, as illustrated in Fig. 3(a1), the superimposed raw BPM data responses of type-1 BPMs generated by a horizontal orbit distortion do not show the same responses, making a calibration necessary.

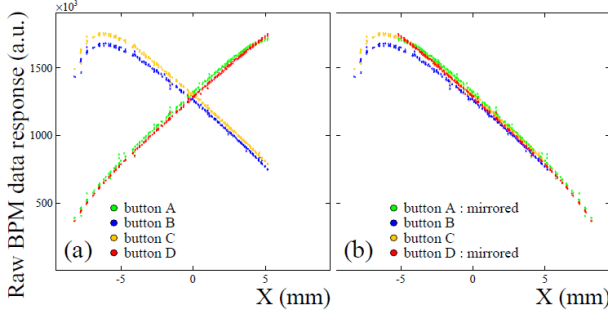


Figure 2: Raw BPM data responses as a function of horizontal beam position from BPM#5. (a) Overlay of four raw BPM data responses; (b) Overlay of the raw BPM data responses from button B, C, mirrored A and mirrored D.

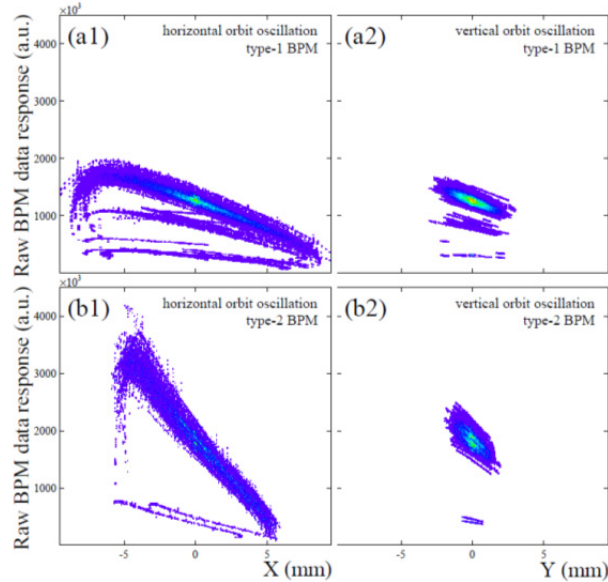


Figure 3: Superimposed raw BPM data responses as a function of horizontal and vertical beam position in the left and right column respectively.

The superimposed raw BPM data responses as a function of horizontal and vertical beam position are shown in the left and right column of Fig. 3, respectively. Plots in the left (right) column of Fig. 3 present the raw BPM data responses generated by a horizontal (vertical) orbit distortion. Plots in the top (bottom) row of Fig. 3 indicate the raw BPM data responses associated with type-1 (type-2) BPMs. Each of four plots in Fig. 3 shows that the superimposed raw BPM data responses consist of one major band plus some outliers located in the low raw BPM data response region. Then, the next step is to

identify and calibrate the outliers whose raw BPM data responses do not lie within the main band for each type. The raw BPM data responses of outliers shown in each of the four plots in Fig. 3 show different slopes and vertical offsets compared to BPMs within the main band. In order to identify those outliers, we apply a line fitting on every raw BPM data response to obtain the slope and vertical offset of individual pickup buttons. Examples are shown in Fig. 4, where line fitting was implemented within ± 3.5 (± 2.2) mm of horizontal (vertical) orbit distortion on type-1 and type-2 BPMs. The fitting boundary was chosen for good and wide linearity for all raw BPM data responses for the same orbit distortion.

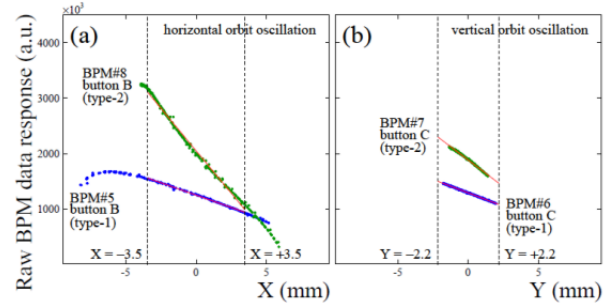


Figure 4: Line fitting (red line) was applied to data points within ± 3.5 mm and ± 2.2 mm in (a) and (b), respectively.

After applying line fitting on every raw BPM data response, we added the fitted slopes and vertical offsets for the same geometry into two separate histograms. A Gaussian fitting of each histogram was then applied to identify normal raw BPM data responses and outliers.

The mean values obtained from a Gaussian fitting of the two histograms are set to be the target values of the calibration. The target of raw BPM data responses is defined in Eq. (3),

$$y_{target} = s_{mean} \cdot x + v_{mean} \quad (3)$$

where y_{target} stands for the target value of the raw BPM data response; x is the horizontal beam position and s_{mean} (v_{mean}) is the mean value for the slope (vertical offset) generated by the Gaussian fitting. For every pickup button, the calibrated raw BPM data response can be interpreted by Eq. (4). The indices (i, j) in the subscript of Eq. (4,5,6) identify the j^{th} button (A/B/C/D) of the i^{th} BPM.

$$g_{i,j} \equiv \frac{s_{mean}}{s_{i,j}} \quad (4)$$

$$v'_{i,j} \equiv v_{mean} - g_{i,j} \cdot v_{i,j} \quad (5)$$

$$y_{cal} = g_{i,j} \cdot y_{i,j} + v'_{i,j} \quad (6)$$

$s_{i,j}$	measured slope
$v_{i,j}$	measured vertical offset
$g_{i,j}$	required gain
$v'_{i,j}$	required vertical offset
$y_{i,j}$	measured raw BPM data response
y_{cal}	Calibrated raw BPM data response

RESULTS AND DISCUSSION

We summarize the fit values of the vertical offsets and slopes for the horizontal orbit distortion in Fig. 5(a1) and (b1), respectively. To compare the results between type-1

and type-2 BPMs, as shown in Fig. 5(b1), we note that the pickup button responses for type-2 BPMs show steeper slopes. This could be explained by geometric differences. Limited vertical space causes the surface charge density to be higher in type-2 BPM pickup electrodes. Moreover, as illustrated in Fig. 5(b1), the fitted slopes of BPMs #111 and #119 reveal relatively large error bars due to larger uncertainty of the response linearity within the fitting range, which can be verified by checking the sweep ranges of horizontal orbit distortions. As shown in Fig. 6, almost no sweep range exists for BPM#111 and #119 making it impossible to perform a correct line fitting.

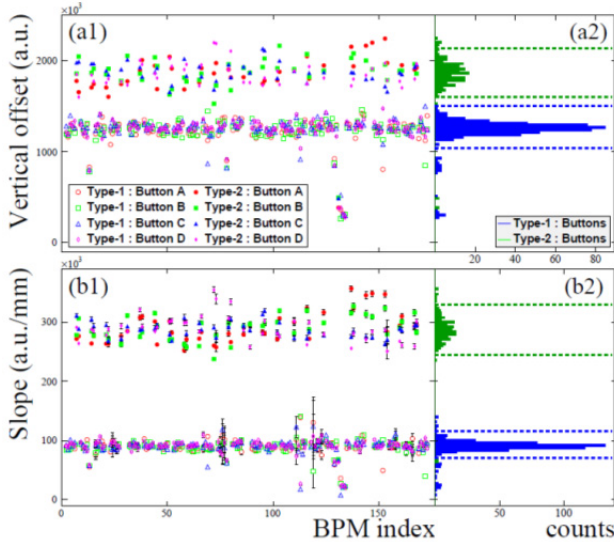


Figure 5: BPM index dependence of fitted vertical offsets and slopes for horizontal orbit distortion is shown in (a1) and (b1) separately, and four associated histograms (two types of BPMs and two kind of fitted results) are superimposed in (a2) and (b2) individually. The legends of (b1) and (b2) are exactly the same as those of (a1) and (a2) respectively.

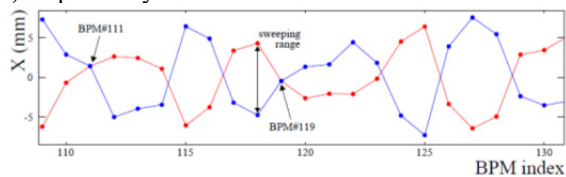


Figure 6: Horizontal beam positions of orbit distortion generated by a horizontal corrector magnet with positive (negative) currents are shown by red (blue) data points. For each BPM index, the distance between the red and blue point indicates the sweep range of this BPM.

While we implement the gain values and vertical offsets on the outliers, the expected raw BPM data responses of the two BPM types are shown in Fig. 7 for horizontal and vertical orbit distortions. Compared with the four plots in Fig. 3, all outliers in each of the four plots in Fig. 7 have been rotated and/or shifted into the main band of raw BPM data responses, as expected. To have a closer look at each plot in Fig. 7, we note that because of the relatively small sweep range on (a2) and (b2) generated by vertical orbit distortions, all raw BPM data responses, with or without calibration, have good

linearity within the sweep range. However, raw BPM data responses generated by horizontal orbit distortions could not be calibrated well while the beam position are outside of the ± 3.5 mm range, where the gain is reduced. Fortunately, since the electron beam at the TPS storage ring usually stays within 1 mm in the transverse plane, this algorithm is applicable. To make a comparison between the calibration results and conditions of the horizontal and vertical orbit distortion, both can provide well-calibrated responses. In case of the TPS storage ring, however, for reliable line fits, a horizontal orbit distortion will be a better choice, since BPMs are installed at more appropriate longitudinal positions to allow wider sweep ranges.

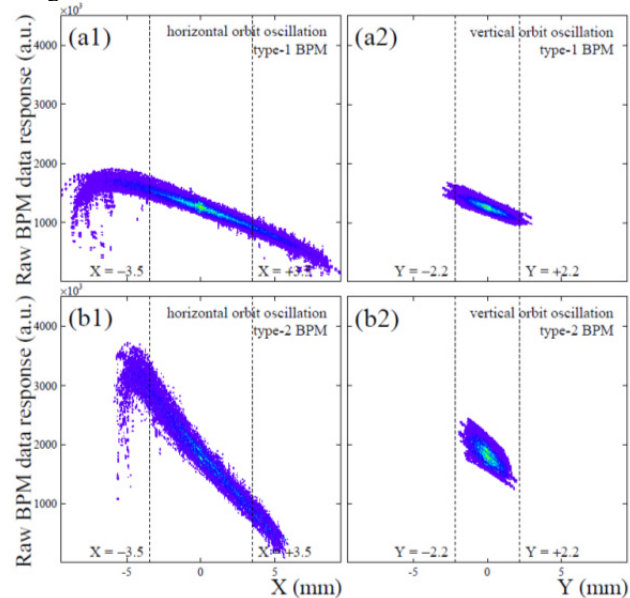


Figure 7: Expected raw calibrated BPM data responses of two types of BPMs for Data d001 and d002. In each plot, only the raw BPM data responses with two vertical-dashed lines are well-calibrated.

SUMMARY

We successfully established a fast gain calibration algorithm for the BPMs. Choosing the proper sweep range, we could identify and calibrate the outliers of pickup buttons well. With this algorithm, we could quickly record and verify the conditions of BPMs, and ensure a stable and reliable operation at modern accelerators. In case of the TPS storage ring, the installed BPMs show a linear response within ± 3.5 (± 2.2) mm in the horizontal and vertical plane. This range is wide enough to safely operate the TPS storage ring, since the electron beam usually orbits within 1 mm of the ideal orbit. We therefore perform the BPM calibration based on the first 10-turn data with horizontal orbit distortion at a beam current of 15 mA in 20 minutes.

REFERENCES

- [1] C. Y. Liao and P. C. Chiu, "TPS Training Course - Basic of Beam Diagnostics", 2014. Unpublished manuscript.
- [2] M. Billing, AIP Conf. Proc., **281**, 55 (1993).